ISSN 0915-633X

NATIONAL INSTITUTE FOR FUSION SCIENCE

An Algorithm to Remove Fringe Jumps and its Application to Microwave Reflectometry

A. Ejiri, K. Shinohara and K. Kawahata

(Received - Mar. 10, 1997)

NIFS-491 Apr. 1997

RESEARCH REPORT
NIFS Series

NAGOYA, JAPAN

An Algorithm to Remove Fringe Jumps and its Application to Microwave Reflectometry

A Ejiri†, K Shinohara‡ and K Kawahata†

† National Institute for Fusion Science, Nagoya 464-01, Japan

‡ Department of Physics, Faculty of Science, University of Tokyo, Tokyo 113, Japan

Abstract. In some plasma discharges the phase measured by microwave reflectometry has many fringe (2π rad.) jumps. A new algorithm to detect and remove fringe jumps has been developed, and applied to the data in the JIPP TII-U tokamak. Using this algorithm, quantitative properties of fringe jumps, and their effects on the analysis of phase fluctuations are investigated. It was found that the fringe jumps occur randomly, and the distribution of the time scale (half period) of jumps has a peak around $4 \sim 6\mu$s. The rms value of high frequency phase fluctuations in fringe jump periods is larger than that in fringe jump-free periods. Besides this high frequency fluctuations, fringe jumps themselves have much smaller power than that of fluctuations in high frequency range. In low frequency range, however, the power spectrum is dominated by the random fringe jumps.

PACS numbers: 57.70.Gw, 52.25.Gj, 02.70.Rw, 02.50.Ey

keywords:algorithm, microwave refletometry, fringe jumps, phase runaway, Poisson process, Power spectrum

Short title: An Algorithm to Remove Fringe Jumps and its Application to Microwave Reflectometry

April 4, 1997

1. Introduction

Microwave reflectometry is a powerful method to measure density profiles and fluctuations in magnetically confined plasmas [1,2,3,4]. Microwaves launched into a plasma are reflected at the cutoff layer of which position is a function of density (for O-mode waves). Measuring the phase of the round trip propagation, we can get information on density profiles and fluctuations. One of the problems in microwave reflectometry is the phase runaway effect, which is the phenomenon that the measured phase moves unreasonably fast in one direction. This phase runaway has been observed by many reflectometers in fusion devices [5,6,7,8,9].

Experimental results in the JIPP T II-U tokamak [10] indicate that the phase runaway is not caused by errors in the measurement system, but is a result of interaction between microwaves and the plasma [7]. Several different types of microwave reflectometers have been used in JIPP T II-U, and phase runaway was observed in all systems. Furthermore, it was found that the runaway is not caused by the effect of noise in the measurements. These results suggest a complicated picture for the reflection layer.

In order to get information on density profiles and density fluctuations, the mechanism of the phase runaway and its effect on the measurements should be investigated. Although there is some inference on the mechanism of phase runaway [5, 9,11], it is not fully understood. The understanding will lead to an appropriate measurement scheme or to an appropriate analysis method.

In this article the data with the following properties are analyzed. In some discharges in JIPP T II-U and JFT-2M, plasma devices, the phase runaway consists of many discrete fringe jumps (i.e. 2π phase differences). Furthermore, the phase behavior besides fringe jumps appears to be reasonable [6,7]. On the other hand, in some other discharges, the runaway seems to be caused by continuous phase running [8].

Automatic removing of fringe jumps has been used in interferometers or even in a reflectometer [6], and it is rather a standard procedure. However, the situations of interferometers and reflectometers are quite different. In interferomters, fringe jumps occur due to noises or due to rapid phase change. Fringe jumps are much faster than the time scale of interest, and they are much larger than the amplitude of phase fluctuations. In addition, they do not occur as freqeuntly as those in reflectometer. As a result, it is not so difficult to remove automatically such fringe jumps which have quite different properties from thoes of the phase behaviour of interest. On the other hand, in reflectometers, the time scale and the amplitude of phase fluctuations are close to those of fringe jumps. A new algorithm to detect and remove fringe jumps has been developed, and applied to reflectometers. Using such an algorithm, not only we can get fringe jump-free phase behavior, but we can investigate quantitative properties of fringe jumps. Those properties will lead to the mechanism of fringe jumps and phase

runaway. In addition, we can address the problem whether the properties of phase after removing fringe jumps are different from those of the original phase. The results may give validity of the analysis we had often used under the influence of fringe jumps. For example, it is assumed that high frequency components of fluctuations are not affected by fringe jumps and phase runaway [5]. In section 2, we describe the principle of the algorithm. The application to the microwave reflectometry is demonstrated in section 3. Using the quantities obtained by the algorithm, the properties of fringe jumps and phase fluctuations are presented in sections 4 and 5, respectively.

2. Principle of the algorithm to remove fringe jumps

Generally the measurement of phase has the ambiguity of an integer fringe ($2\pi n$, where n is an integer). Thus, the first procedure in analysis is to fix the ambiguity and connect each data point. This is an inevitable procedure for almost all phase measurements. In a time series of phase, the possibilities of $0, \pm 2\pi$ phase ambiguity is checked, and the phase which yields the minimum phase change from the previous phase is selected (figure 1). This connected phase is subsequently referred to as the original phase, and this procedure as the phase connection process. In order to avoid misconnection the phase should be sampled with a time interval shorter than the time scale of phase movement. All further analysis is applied to the original phase.

A schematic time behavior of a fringe jump after the initial phase connection process is shown in figure 2(a). In a long time scale, the phase has a fringe jump (2π phase difference). In a short time scale (during a fringe jump), however, the phase changes gradually. The phase also has fast fluctuations, in which we are interested. The measured data include many fringe jumps. Furthermore, the time scales of each fringe jump are not the same. Thus, a new algorithm to detect and remove each fringe jump automatically is required.

The basic pattern of a fringe jump can be represented as being constant before and after the fringe jump, and having a linear 2π change during the jump (line CABD in figure 2(a)). The algorithm has the following four steps: (i) The timing of a fringe jump (time $(t_A + t_B)/2$ in figure 2(a)) is detected. (ii) The width $(t_A - t_B)$ is determined for each fringe jump. Note that the width may be different for each fringe jump. The data points during the fringe jump ($t_A \sim t_B$) are skipped. (iii) After skipping fringe jumps the residual phase (data points) are connected using the same method as the initial phase connection process. Since the data before and after a fringe jump have the difference of about 2π, the jump is removed by the phase connection process (figure 2(b)). (iv) The skipped data are reconstructed from the original data. We assume that the phase during a fringe jump is the superposition of a linear 2π change and fluctuations.

Here the step (i) and (ii) are described using a negative-going fringe jump written

as

$$f(t) \;=\; \bar{f} + f_0(t, w_f) + \tilde{f}(t)\ , \tag{1}$$

where $\bar{f}$ is the time averaged component, and $f_0(t, w_f)$ is the basic pattern of a fringe jump, which is modeled as

$$f_0(t, w_f) \;=\; \begin{cases} +\pi & t \le -w_f \\ -\pi t/w_f & -w_f \le t < +w_f \\ -\pi & t \ge +w_f \end{cases}\ ,$$

where $w_f > 0$ is the half period of the fringe jump. w_f is a free parameter which characterize fringe jumps, and it could take different values for each fringe jump. $\tilde{f}(t)$ is the remaining component, which fluctuates around the basic pattern. The algorithm is explained for a negative-going fringe jump, and the case for a positive-going one follow the same procedure except some signs in equations. We recognize a fringe jump when the period of the jump is much shorter than the periods being almost constant before and after the jump. A natural numerical method to detect a fringe jump is to convolute the phase signal with a kernel which has a similar time behavior as the fringe jump (figure 3). The kernel function $g(t, w_k)$ is defined as

$$g(t, w_k) \;=\; \begin{cases} +1/2\pi w_k & -w_k < t < 0 \\ -1/2\pi w_k & 0 < t < +w_k \\ 0 & t < -w_k, t > +w_k \end{cases}\ ,$$

where $w_k > 0$ is the width of the kernel function. The convolution of $f(t)$ and $g(t, w_k)$ is written as

$$\begin{aligned} p(s, w_k) \;&\equiv\; \int dt f(t) g(t - s, w_k) \\ &=\; \int dt \left(f_0(t, w_f) + \tilde{f}(t) \right) g(t - s, w_k) \\ &=\; \frac{1}{2\pi w_k} \int_{s-w_k}^{s} dt \left(f_0(t, w_f) + \tilde{f}(t) \right) - \frac{1}{2\pi w_k} \int_{s}^{s+w_k} dt \left(f_0(t, w_f) + \tilde{f}(t) \right) \\ &=\; \frac{1}{2\pi w_k} \left(\int_{s-w_k}^{s} dt f_0(t, w_f) - \int_{s}^{s+w_k} dt f_0(t, w_f) \right) \\ &\quad + \frac{1}{2\pi w_k} \left(\overline{\tilde{f}(t)}|_{s-w_k<t<s} - \overline{\tilde{f}(t)}|_{s<t<s+w_k} \right)\ . \end{aligned} \tag{2}$$

The second term is expected to be very small, because $|\overline{\tilde{f}(t)}| \ll \pi$. The first term has a peak at $s = 0$. The convolution is normalized, so that the peak height for the stepwise fringe jump ($f_0(t, w_f = 0)$) is 1. The convolution shows a positive peak for a negative-going fringe jump and a negative peak for a positive-going fringe jump. Each peak (fringe jump) can be detected by an appropriate threshold level in the convolution (figure 3).

The convolution of the basic pattern $f_0(t, w_f)$ and the kernel function consists of linear parts and parabolic curves. If the time is normalized to w_k, the convolution $(p(s, w_k, w_f))$ becomes a function of $w_f/w_k(\equiv \alpha)$ (figure 4). The peak height is written as $1 - \alpha/2$, and the height decreases with the increase of α. The width of the fringe jump $f_0(t, w_f)$ is α by definition. Let us consider the case w_k and α are given. When the threshold level is set to be $\pm(1 - \alpha/2)$, we can detect fringe jumps with w_f shorter than αw_k. Then we skip the data in the time window $|t - t_{peak}| < \alpha w_k$, where t_{peak} is the time of the peak.

When the time scale of a fringe jump is shorter than αw_k, this method skips not only the data points during the fringe jump, but also extra data points outside the fringe jump period. In order to minimize this over-skipping, the fringe jumps with almost same w_f are detected and skipped at one time. This is realized by increasing w_k step by step. In this procedure, faster jumps (i.e. smaller w_f) are removed earlier, and slower jumps (i.e. larger w_f) are removed later. The kernel width w_k is increased gradually. At each step, fringe jumps with $w_f \approx \alpha w_k$ are detected and skipped. The fringe jumps with shorter w_f are already skipped in the previous steps. In our case, w_k is increased from 6 to 450μs. This range corresponds to 2 to 150μs in $w_f = \alpha w_k$. α is fixed to be 1/3. This value implies that the algorithm finds a fringe jump which has at least twice longer constant period than the period of the fringe jump. At each w_k, fringe jumps are detected and the data during jumps are removed (skipped).

The next processes are the steps (iii) and (iv). After removing all fringe jumps, the residual phase consists of many fragments interrupted by fringe jumps. The phase in each fragment includes no fringe jumps. Each successive fragments have almost integer fringe difference (i.e. $2n\pi$). These residual phase are connected using the phase connection process, so that the connected phase include no fringe jumps. The data during fringe jumps, which are skipped in the step (ii), are reconstructed as follows: The linear trend during each fringe jump is calculated, and the trend is subtracted from the original data. This reconstructed data do not have fringe jumps, and are connected smoothly to the residual phase (figure 2).

Here we summarize briefly the concept of this algorithm and describe possible problems we would encounter. When we recognize a fringe jump by our eyes, the phase shows a jump of integer fringe, and the time scale of the jump is relatively shorter the periods of constant phase before and after the jump. The main component of fringe jumps is expressed as $f_0(t, w_f)$. The algorithm finds this pattern by the convolution of phase with the stepwise function $g(t, w_k)$. This is a kind of wavelet transform [12]. Since the algorithm can detect fringe jumps automatically, it might be usefull for other phase measurements. For instance, the algorithm can be applied to interferometers. They could suffer from fringe jumps due to small probing beam power, or due to spikes caused by X-rays in their signals.

Although we reconstruct the data during jumps, we do not know whether the properties of fluctuations of residual phase are the same as those of the data during fringe jumps. Thus, a comparison of characteristics of fluctuations in fringe jump periods and those in fringe jump-free periods is required.

3. Application to microwave reflectometry

This algorithm has been applied to the data of a microwave reflectometer in the JIPPT II-U tokamak. A Gunn oscillator with the frequency of 57GHz is used as a probing microwave source, and a backward oscillator is used as a local oscillator. The X-mode microwave is launched into the plasma and reflected at the cutoff layer at the plasma edge. The reflected wave is measured by a heterodyne system. The beat frequency is about 1.1GHz, and it is down-converted to 880MHz by a feed forward tracking receiver [13]. The phase of 880MHz signals is measured by a sine-cosine detector. The detector yields two outputs which are proportional to the sine and cosine components, respectively. The signals are sampled by an ADC with the time interval of 1μs. The phase and the amplitude of the reflected wave are measured, and the signal to noise ratio can be monitored. More information on the experiments will be available in [7]. In some discharges, we can observe many fringe jumps by our eyes (figure 5), and the algorithm is applied to such data. In other discharges, we cannot identify fringe jumps by our eyes, and the application of the algorithm might be meaningless.

Figure 6 shows the fringe jumps detected at a step in the increasing w_k. Fringe jumps with $w_f \leq \alpha w_k$ are detected by the threshold of $\pm(1-\alpha/2) = \pm 5/6$ in the convolution. Since faster fringe jumps are already removed, only the fringe jumps with $w_f \approx \alpha w_k$ are detected at this step. The data points in the time window $|t - t_{peak}| < \alpha w_k = w_f$ are skipped. The experimental fringe jumps in this step, fluctuate around the basic pattern (dotted lines in figure 6(a)), so that the linear approximation for phase change during a fringe jump seems to be reasonable. The jumps with long w_f, however, deviate from the line. Figure 7 shows the phase as a function of normalized time for short and long w_f. Each dot represents one time sample, and data from four similar discharges are plotted. While the phase with $w_f \leq 10\mu$s shows a linear change during jumps, the phase with longer w_f appears to be represented by three-fold lines. The phase has a fast change at the middle of the fringe jump, and slow change at the start and end of the jump. This deviation from the line could cause errors in the timing and time scale of a fringe jump.

Figure 8 shows the ratio of residual data points to the total points (a), number of detected fringe jumps (b) and square average of the convolution (c) as a function of w_f, which corresponds to each step in the increasing w_k. As we increase w_k, more fringe jumps are removed, so that the ratio of residual data decreases. All fringe jumps within the time window of 30ms are removed when w_f is increased up to 100μs, and

the final ratio of residual data points, which exist in fringe jump-free periods, is 85%. The other 15% are data points during fringe jumps. $\overline{p^2}$ is a measure of fringe jumps. Each fringe jump causes a peak in p, so that $\overline{p^2}$ decreases as the number of fringe jumps decreases. When fringe jumps are detected at certain w_k, $\overline{p^2}$ drops (e.g. arrows in Fig. 8). After removing all fringe jumps, $\overline{p^2}$ stays almost constant, which arises from phase fluctuations.

Figure 5 shows a part of time behaviors of the original phase and the corrected phase. While the original phase includes several fringe jumps, all those are removed by the algorithm in the corrected data. During the whole measurement of about 200 ms, the original phase moves more than 1000 rad. On the other hand, the corrected phase (after removing fringe jumps) moves about 20 rad. The corrected phase still includes several fringe jumps which could not be removed by the algorithm. These fringe jumps have relatively long time scale, and it is difficult to distinguish such slow fringe jumps from the time variation of the phase. In this experiment, the plasma edge is measured, so that the phase is expected to represent the movement of the edge, rather than the density variation. The slow behavior of the corrected phase seems to be reasonable. Thus, we can conclude that the data points in fringe jump-free periods represent macroscopic movement of the cutoff layer. From these results of the application, it is shown that the algorithm is a powerful tool to detect and remove fringe jumps. In addition, the algorithm produces many interesting quantities. In the following section, the data set of 30ms long, which includes the data figure 5, is analyzed. In some analysis, four similar data sets are used to reduce statitical errors.

4. Properties of the fringe jumps

By using the algorithm we get two quantities for each fringe jump. One is the occurrence time , and the other is the time scale w_f. When we can assume that the time scale w_f is much shorter than the typical time between successive fringe jumps, these fringe jumps are classified as a marked point process. Fringe jumps are events on time, and have a mark w_f for each event. In this section, we show the properties of occurrence time and w_f from the view point of a marked point process.

The simplest model for a random point process is the stationary Poisson process. In this process, each occurrence is independent and the mean rate λ that events occur is a constant. It is the only parameter for the process. As a counting process, the counts in period T obey the Poisson distribution with the mean counts of λT. Consider the case we observe n events in an interval T and measure the interarrival time, which is the time between two successive events. Let N be the number of interarrival times of duration exceeding τ. Then the expectation of N is

$$\mathrm{E}[N(\tau)] = ne^{-\lambda\tau} . \tag{3}$$

This negative exponential arises from independence property of the stationary Poisson process. The distribution function of the interarrival time, namely the derivative of (3) with τ. also has an exponential decay.

Figure 9 shows the number $N(\tau)$ defined above for observed fringe jumps in 30ms time window of a discharge. $N(\tau)$ decreases exponentially with τ. As a test for a stationary Poisson process, the $\pm\sigma_N$ range is also plotted in the figure. The range is calculated as [14]

$$\mathrm{E}[N(\tau)] \pm \sigma_N = \mathrm{E}[N(\tau)] \left(1 \pm \sqrt{\frac{1 - e^{-\lambda\tau}}{ne^{-\lambda\tau}}} \right) . \tag{4}$$

For λ, we took the measured mean rate, which is the best estimation for a given number of counts. The observed points are distributed in the range $\pm\sigma_N$ except the points around $\tau = 1$ms, which represent one interarrival time (fringe jump). We can conclude that the fringe jump occurrence obeys a stationary Poisson process within the statistical error. This implies that the fringe jump occurrence is random and show neither periodicity nor clustering.

Figure 10 shows the distribution of the time scale w_f of positive and negative-going fringe jumps. Four data sets with the mean rate of $2.6 \sim 3.7$jumps/ms is accumulated to reduce the statistical error. It has a peak at $w_f = 4 \sim 6\mu$s, and decreases gradually with w_f. It should be noted that the number of fringe jumps seems to decrease as w_f decreases to zero. If it has an infinite peak at $w_f = 0$. then it is impossible to detect all fringe jumps even though we measure the phase with very fast measurement system. In our case, the minimum detectable time scale is $w_f \sim 1\mu$s, which is the sampling time. This property is very important for practical measurements. The distributions of positive and negative-going fringe jumps are different. The negative-going one is extended to longer time scale, and the total number of fringe jumps is smaller than that of positive-going jumps.

The relation between the interarrival time and the time scale w_f is not clear. When we plot w_f as a function of forward or backward interarrival times, there seems to be neither positive nor negative correlation between them. The marked-point process is classified as a compound Poisson process when the interarrival times (or occurrence time) and the mark w_f are independent [15]. This process can be represented as a superposition of independent Poisson processes, and each process has different w_f.

The facts that fringe jumps occur randomly and that the time scale of jumps distributed over wide range imply that the fringe jumps are caused by neither a periodic (in time-domain) structure nor a regular (in spatial-domain) one. A two-dimensional simulation of the propagation of microwaves has demonstrated that periodic unidirectional phase change (fringe jumps) can be caused by a regular perturbation moving perpendicular to the direction of microwave propagation [11]. On the other

hand, the experimental fringe jumps are not periodic. Moreover, the experimental phase has both positive and negative fringe jumps. Obtained properties of fringe jumps suggest the existence of much more stochastic structure.

5. Phase fluctuations

When we use a microwave reflectometer, we expect that the measured phase include the information on density fluctuations in plasmas. In this section, the properties of phase fluctuations and effects of fringe jumps will be shown. One of the issues is the difference between the properties of fluctuations during fringe jump and fringe jump-free periods. To clarify the difference we calculate root-mean-square (rms) values, distributions of phase increment and power spectra.

Since the time scale of fringe jumps is rather short, the time window for the calculation of rms values should be shorter than the period of fringe jumps. A linear trend is subtracted before calculating rms values, because the phase during jumps have an obvious linear phase change. Fringe jumps with $w_f = 8 \sim 10\mu$s are selected for the calculation, because the phase with longer w_f deviates clearly from a linear relation (figure 7(c),(d)). Then the time widow for the calculation is set to be $18\mu\text{s} \approx 2w_f$. This rms value represents the amplitude of fluctuations with the frequency higher than about 50kHz. The same procedure is used to calculate rms values in fringe jump-free periods, and time windows which are far from fringe jumps are selected to avoid possible effects of the fringe jumps. Figure 11 shows the distributions of rms values for the phase fluctuations in fringe jump-free and fringe jump periods. It is clearly seen that the former is distributed at smaller rms values, while the latter one is distributed over wide range of rms values. The average rms value during fringe jumps is about twice larger than that for fringe jump-free periods.

Phase increment between two consecutive data points, which have 1μs difference in measurement time, represents short term properties of the fluctuations. Figure 12 shows the distribution of phase increment during positive and negative-going fringe jumps, and that for fringe jump-free periods. The last one has a narrowest symmetric distribution, and the distribution at large phase increment has the power law of $\Delta\phi^{-2.7}$ (figure 12(b)). On the other hand, the distributions during fringe jumps are asymmetric. In the case of positive-going fringe jumps, the slope in positive $\Delta\phi$ is much larger than the symmetric distribution, but the slope in negative $\Delta\phi$ is close to the symmetric one. The distribution for the negative-going jumps follow the symmetric one in positive $\Delta\phi$, and it is lager than the symmetric one in negative $\Delta\phi$. It is notable that these asymmetric distributions are not a simple positive nor a negative shift (i.e. Doppler shift) of a symmetric distribution. Thus, the fringe jumps cannot be attributed to a simple movement of the cutoff layer along the direction of microwave propagation (i.e.

radial direction).

The power spectra of the original phase and the corrected phase are calculated. While many fringe jumps exist in the former, basic patterns of fringe jumps are removed in the latter. As illustrated in figure 2, fluctuating components are included in both original and corrected phase. The spectrum of original phase has much larger power than that of the corrected phase in low frequency range (figure 13). This large power is due to the random fringe jumps. The difference decreases gradually with frequency. In order to clarify the effect of (the basic patterns of) fringe jumps, we simulate a phase with fringe jumps (figure 14), of which number and time scale are the same as those appear in the original phase of figure 5. The simulated phase does not have any fluctuations, and the occurence of the jumps are distributed randomly on time. We can also simulate a phase with stepwise ($w_f = 0$) fringe jumps. Figure 15(a) shows the spectra of simulated phases and that of the original phase. To decrease the statistical error in power, 25 spectra of simulated phases are averaged. These three spectra show almost same power at the frequencies lower than about 10kHz. Thus, the low frequency spectrum of the original phase is dominated by the random fringe jumps. On the other hand, they start to diverge as the frequency goes higher. The power of the simulated phase is lower than that of the original phase, and their difference coinside with the power spectrum of the corrected phase (figure 15(b)). As a result, we can coclude the power spectrum of original phase is the summation of that of corrected phase and that arises from basic patterns of fringe jumps. In other words, the power spectrum of the corrected phase represents that of fluctuations, and the effect of fringe jumps themselves is small in the corrected phase. The power of the simulated phase with stepwise fringe jumps has the largest power near the high frequency limit (figure 15(a)), because a stepwise change include very high frequency components.

6. Conclusions

A new algorithm to detect and remove fringe jumps has been developed. It can be applied to phase measurements, such as reflectometers and interferometers. It was also found to be a very powerful tool to investigate quantitative properties of fringe jumps. The application to microwave reflectometry in JIPP TII-U revealed the following results. The fringe jumps occurs randomly, and the time scale of jumps distributes over wide range. These properties indicate that fringe jumps are not caused by a movement of regular perturbations. Fringe jumps affect the frequency components of phase fluctuations. The rms values of high frequency phase fluctuations during fringe jumps are larger than those in fringe jump-free periods. The low frequency components in the original phase are greatly enhanced by random positive and negative-going fringe jumps. On the other hand, the power spectrum of corrected phase was found to represent that

of fluctuations, and the effect of fringe jumps themselves on the spectrum is excluded. The distributions of phase increment for positive and negative-going fringe jumps are asymmetric, and they are different from the symmetric distribution for fringe jump-free periods. These properties indicate that the plasma has very stochastic perturbations.

Acknowledgments

The authors wish to thank M. Hirsch and K. Itoh for their encouragement. They are also grateful to the JIPP TII-U staff for the supports during the experiments.

References

[1] Simonet F 1985 *Rev. Sci. Instrum.* **56** 664

[2] Hutchinson I H 1987 *Principles of plasma diagnostics* (Cambridge: Cambridge University Press)

[3] Hugenholtz C A J 1990 *Rijnhuizen Report* 90-192

[4] Manso M E 1993 *Plasma Phys. Control. Fusion* **35** B141

[5] Hanson G R, et al. 1992 *Nucl. Fusion* **32** 1593

[6] Sips A C C and Kramer G J 1993 *Plasma Phys. Control. Fusion* **35** 743

[7] Ejiri A. Kawahata K. Tanaka K and JIPP TII-U group 1997 *Fusion Eng. Design* (to be published)

[8] Shinohara K et.al 1997 *Fusion Eng. Design* (to be published)

[9] Branas B. Hirsch M, Bldzuhn J. Estrada T Geist T, Hartfuss H J, Sanchez J and Zhuravlev V 1996 *Proc. 23th Europ. Conf. Plasma Phys. Control Fusion* **20** 1003

[10] K.Toi, et al. 1991 *Proc. 13th Conf. Plasma Physics and Controlled Nuclear Fusion Research, Washington,D.C.* Vol 1 301

[11] Irby J H, Horne A and Stek P C 1993 *Plasma Phys. Control. Fusion* **35** 601

[12] e.g. Holschneider M 1995 *Wavelets* (Oxford: Oxford University Press)

[13] e.g. Done J L 1980 Broadband superheterodyne tracking circuits for millimeter-wave measurements. *Rev. Sci. Instrum.* **51** 317. Hartfuss H J, et al. 1994 *Rev. Sci. Instrum.* **65** 2284

[14] Synder D L 1975 *Random point process* (New York: John Wiley & Sons) p115

[15] e g Parzen E 1964 *Stochastic Processes* (San Francisco: Holden-Day)

Figure captions

Figure 1. Schematic drawing of the phase connection process. When the phase crosses $(2n \pm 1)\pi n$, following phase data are shifted by $\pm 2\pi$ to get continuous phase.

Figure 2. Schematic time behavior of phase with a fringe jump (a), and that after removing the fringe jump (b). The former and the latter are referred to as the original phase and the corrected one, respectively. Open circles repersent the reconstructed phase, which existed in the period of fringe jump

Figure 3. Basic pattern of a fringe jump, kernel function, and their convolution. t_A and t_B are the start and the stop timings of a fringe jump.

Figure 4. Convoultion of $f_0(t, w_f)$ and $g(t, w_k)$. The time is normalized to w_k. This plot shows the case $w_f < 1/2\ w_k$.

Fig.14
Fig.15

Figure 5. Experimental time behavior of original phase (solid line), and corrected phase (dotted line). The original phase includes many fringe jumps.

Figure 6. Fringe jumps (a) detected at a step in the increasing w_k. In this case, $w_k = 18\mu$s. The convolution and threshold are also shown in (b). Both positive-going and negative-going fringe jumps are overplotted by shifting each fringe jump by t_{peak}. The time range $2w_k$ and $2w_f = \alpha w_k$ are indicated by dashed lines. The dotted lines show the case for the fringe jump of the bassic pattern.

Figure 7. Phase evolution during fringe jumps for shorter and longer w_f and for different directions. The time scale is normalized to w_f. The straight lines are line for the basic pattern of the fringe jump, which changes linearly from $\pm\pi$ to $\mp\pi$.

Figure 8. Ratio of residual data points (a), number of detected fringe jumps (b) and square average of convolution $\overline{p^2}$ (c) as a function of w_f. The arrows show one of the steps where a fringe jump is detected and removed.

Figure 9. Number of interarrival times of duration exceeding τ, where τ is an interarrival time. The solid curves show the $\pm\sigma$ range for the stationary Poisson process with the mean rate $\lambda = 103$[Count]/30[ms].

Figure 10. Distribution of the time scale w_f for positive- and negative-going fringe jumps.

Figure 11. Distribution of rms valuses for fringe jump-free periods (a) and for periods of fringe jumps (b).

Figure 12. Distribution of phase increment during positive-going (filled circles) and negative-going (open circles) fringe jumps, and that for fringe jump-free periods (solid curve). The peak height is normalized to be about one. Distributions are shown as a function of Δo (a) and $|\Delta o|$ (b).

Figure 13. Power spectra of original phase (solid curve) and corrected phase (dotted curve).

Figure 14. Simulated time behavior of a phase with the fringe jumps, of which number and time scale are the same as those appear in the original phase of figure 5.

Figure 15. Figure (a) shows power spectra of the simulated phases (with fringe jumps and stepwise fringe jumps) and that of the original phase. The open circles in figure (b) represent the difference between the power of original phase and that of the simulated phase with fringe jumps. The error bars arises from the statistical error of the power of the original phase. The power spectrum of corrected phase is also shown in figure (b).

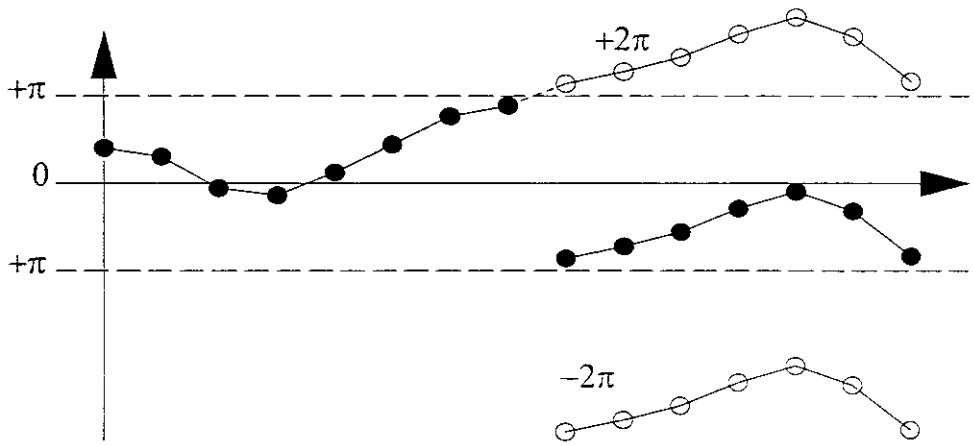
+2π
+π
0
+π
−2π

Fig.1

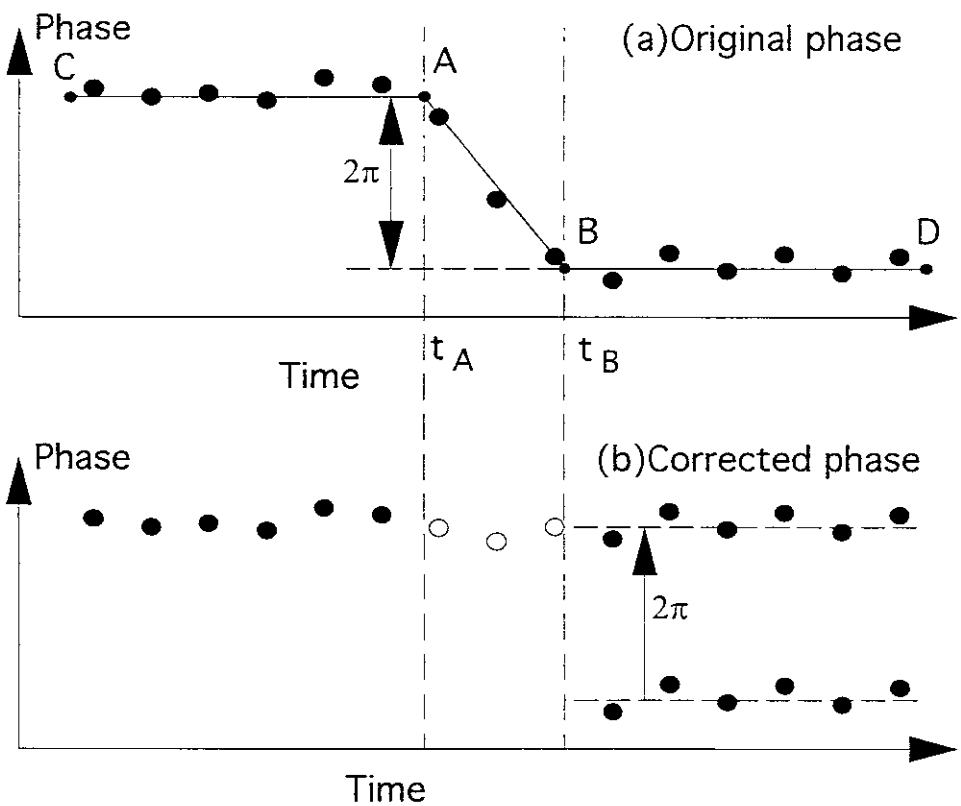
Phase
C
A
(a)Original phase
2π
B
D
t A
t B
Time
Phase
(b)Corrected phase
2π
Time

Fig.2

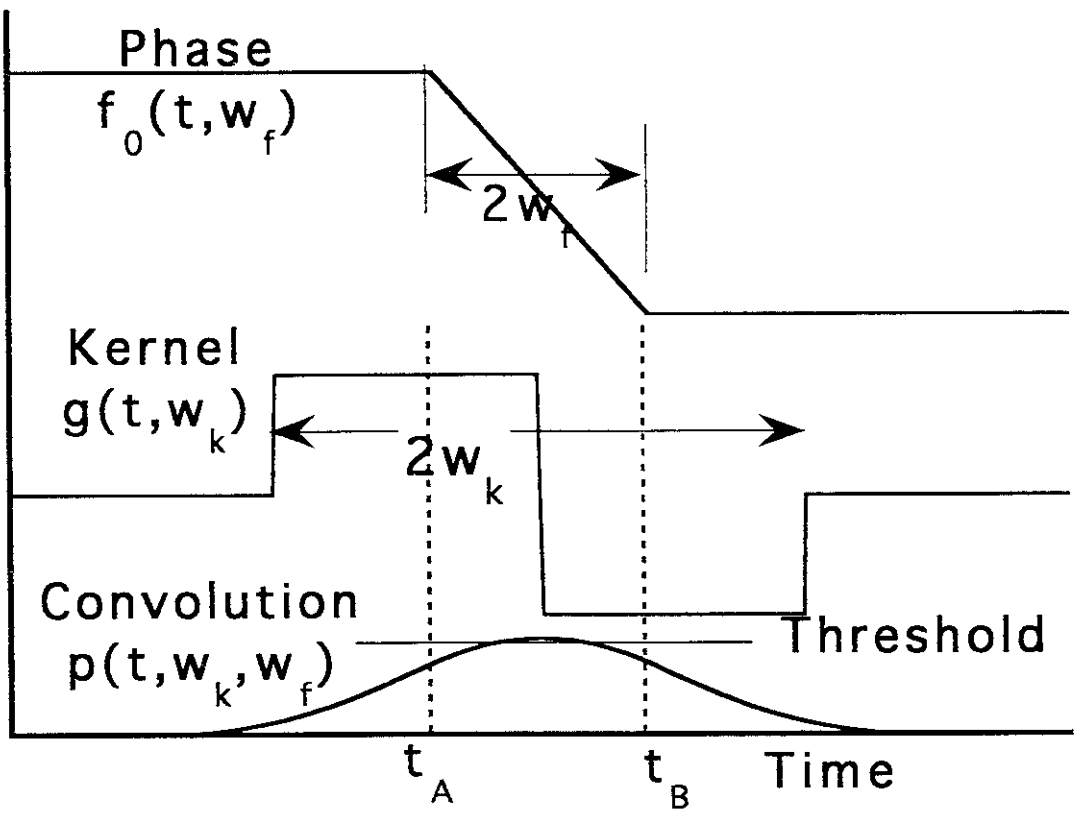
Phase
$f_0(t,w_f)$
$2w_f$
Kernel
$g(t,w_k)$
$2w_k$
Convolution
$p(t,w_k,w_f)$
Threshold
t_A
t_B
Time

Fig. 3

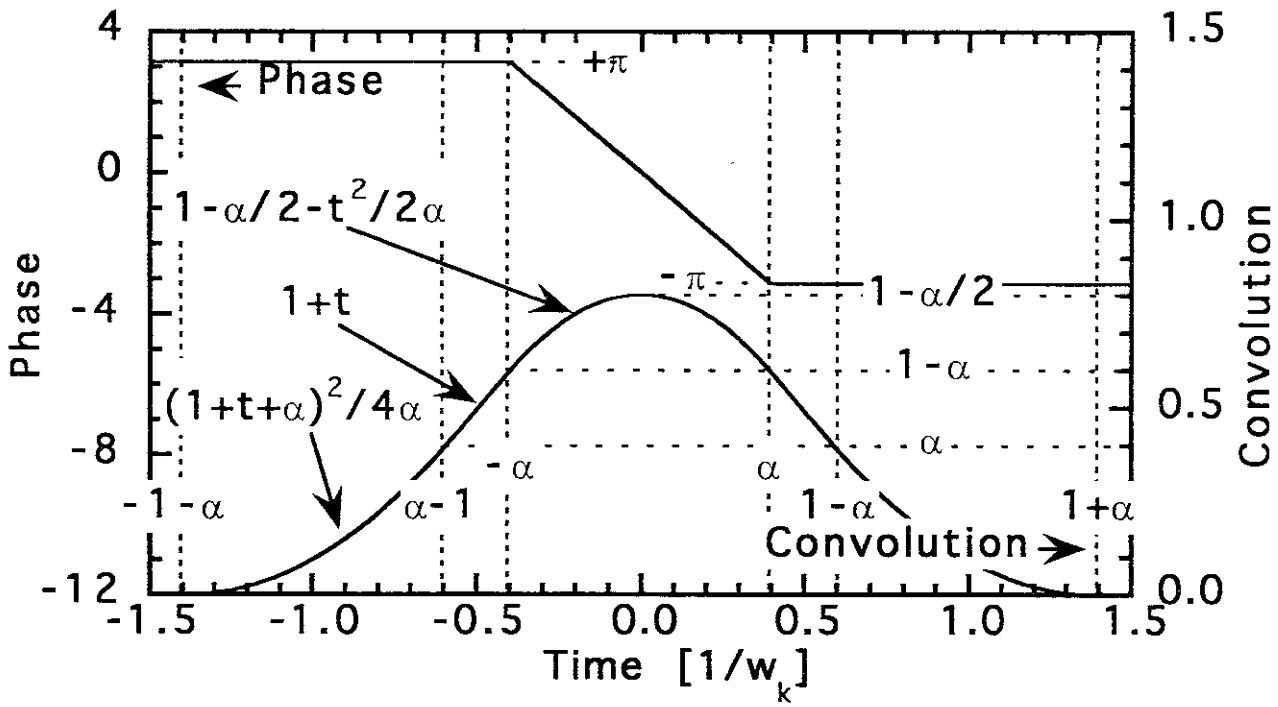
4
0
-4
-8
-12
Phase
1.5
1.0
0.5
0.0
Convolution
-1.5
-1.0
-0.5
0.0
0.5
1.0
1.5
Time [1/w_k]
Phase
+π
-π
1-α/2-t²/2α
1+t
(1+t+α)²/4α
1-α/2
1-α
α
-α
-1-α
α-1
1-α
1+α
Convolution

Fig.4

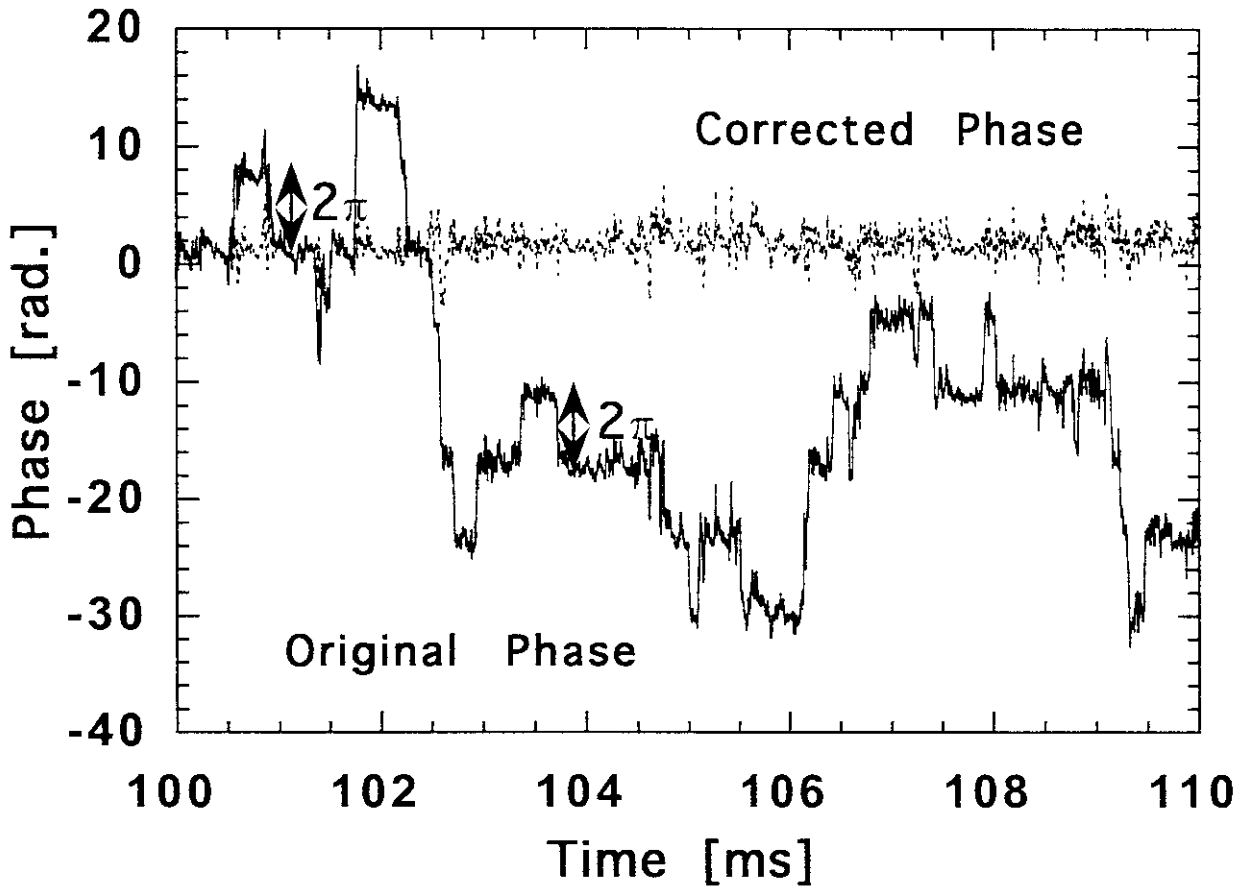
20
10
0
-10
-20
-30
-40
Phase [rad.]
100
102
104
106
108
110
Time [ms]
Corrected Phase
Original Phase
2π
2π

Fig. 5

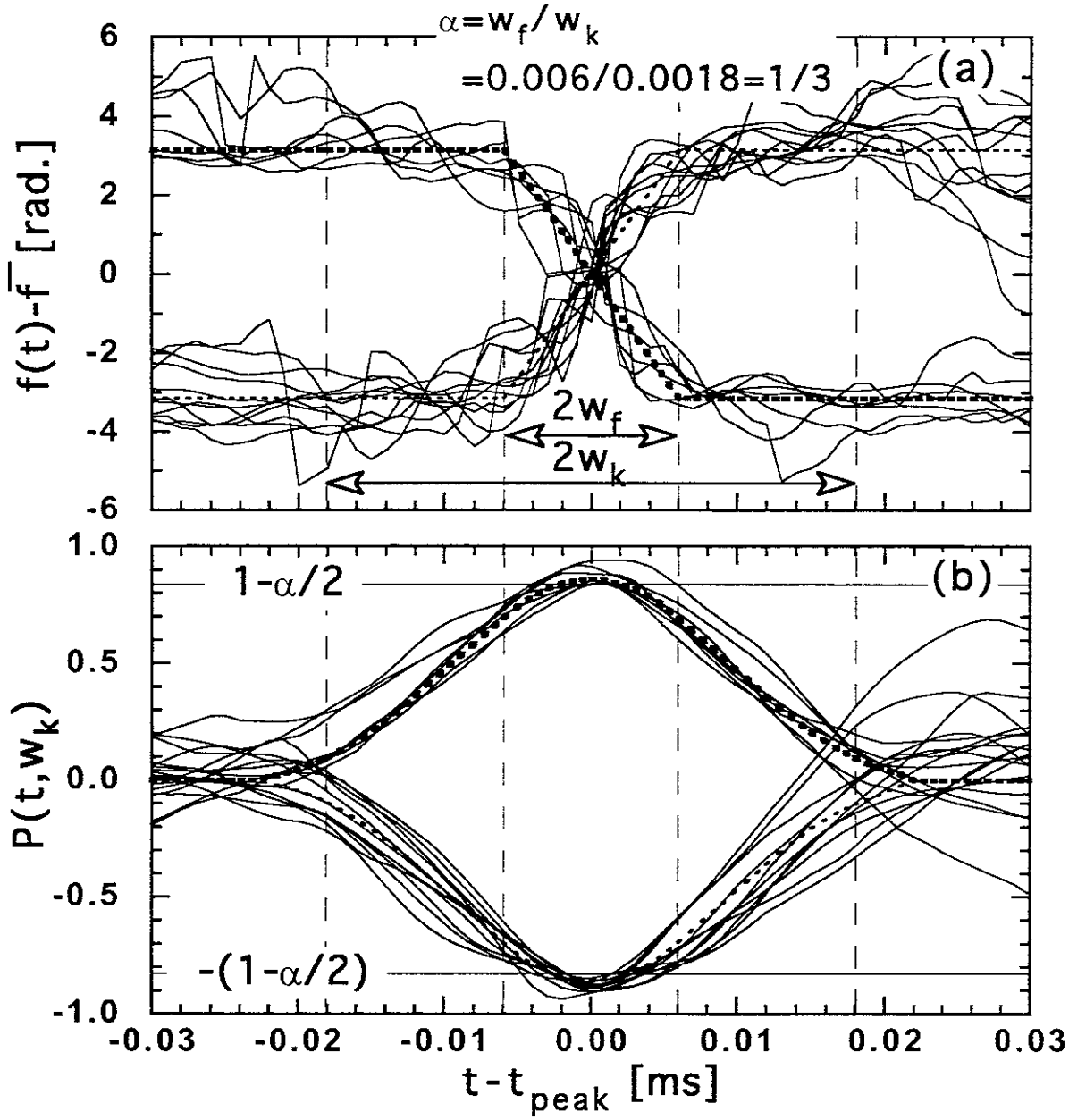

Fig.6

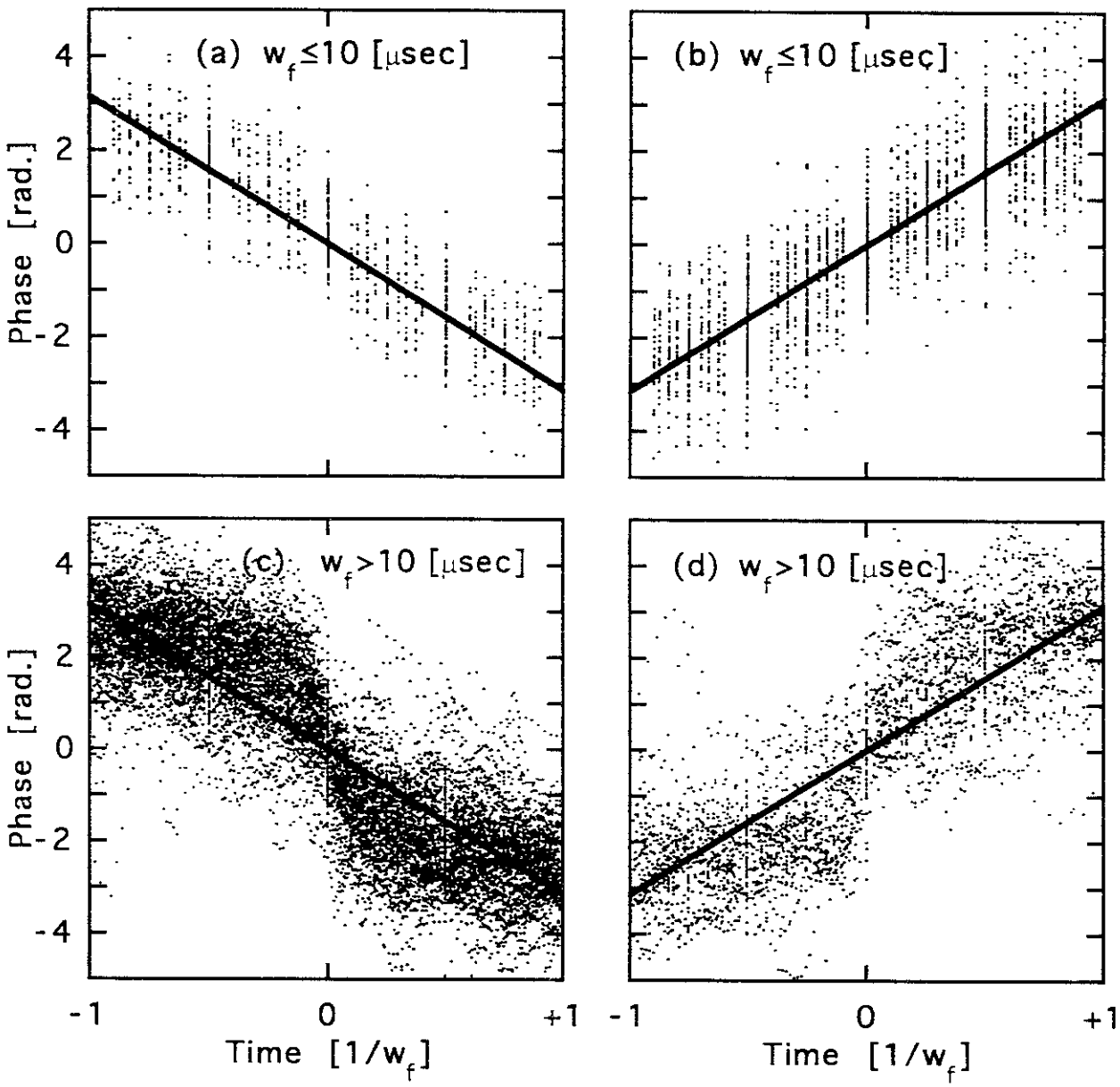
(a) $w_f \leq 10$ [μsec]
(b) $w_f \leq 10$ [μsec]
(c) $w_f > 10$ [μsec]
(d) $w_f > 10$ [μsec]
Phase [rad.]
4
2
0
-2
-4
-1
0
+1
Time [$1/w_f$]

Fig.7

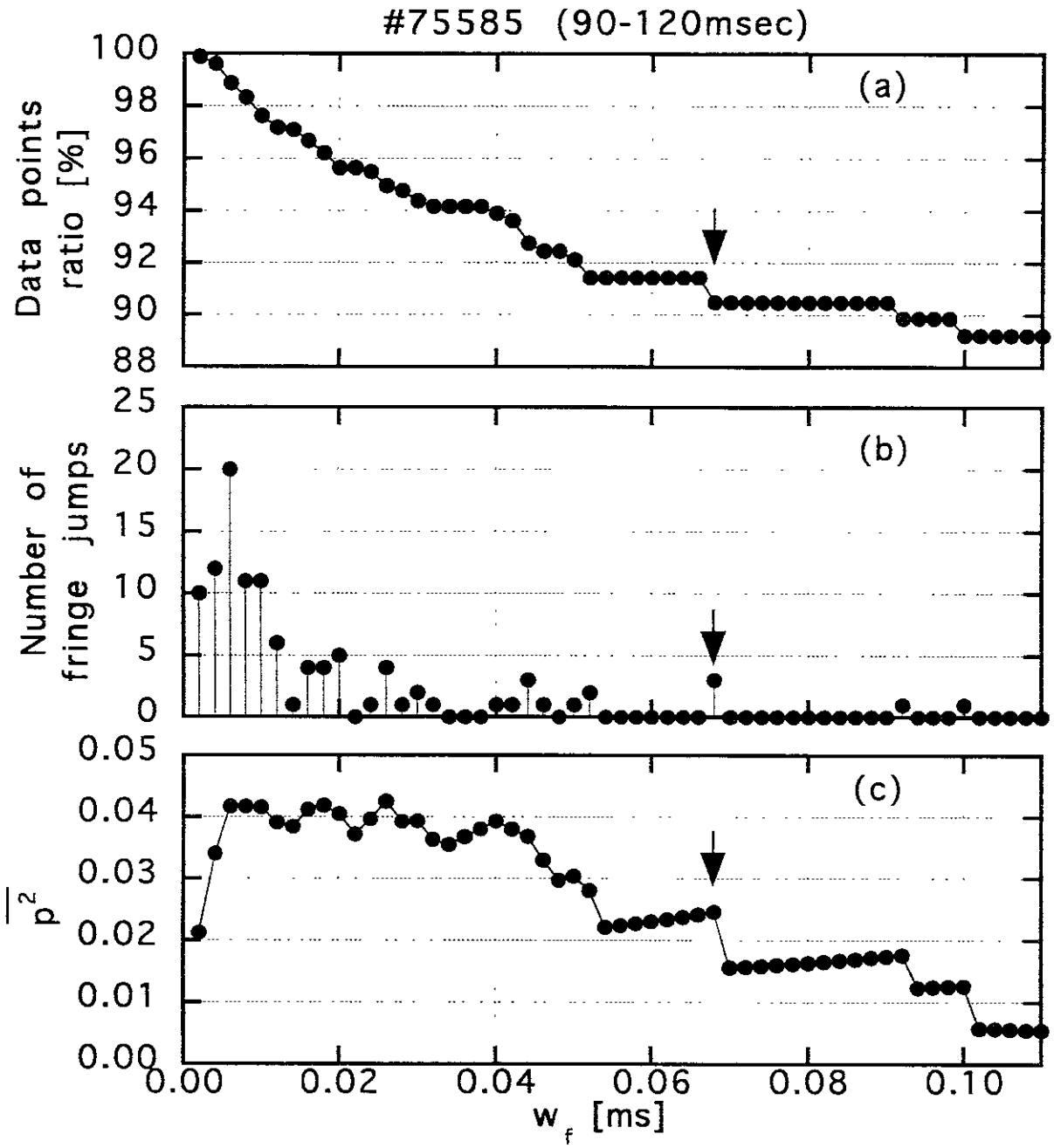
#75585 (90-120msec)
(a)
(b)
(c)
Data points ratio [%]
Number of fringe jumps
$\overline{p^2}$
w_f [ms]
100
98
96
94
92
90
88
25
20
15
10
5
0
0.05
0.04
0.03
0.02
0.01
0.00
0.00
0.02
0.04
0.06
0.08
0.10

Fig.8

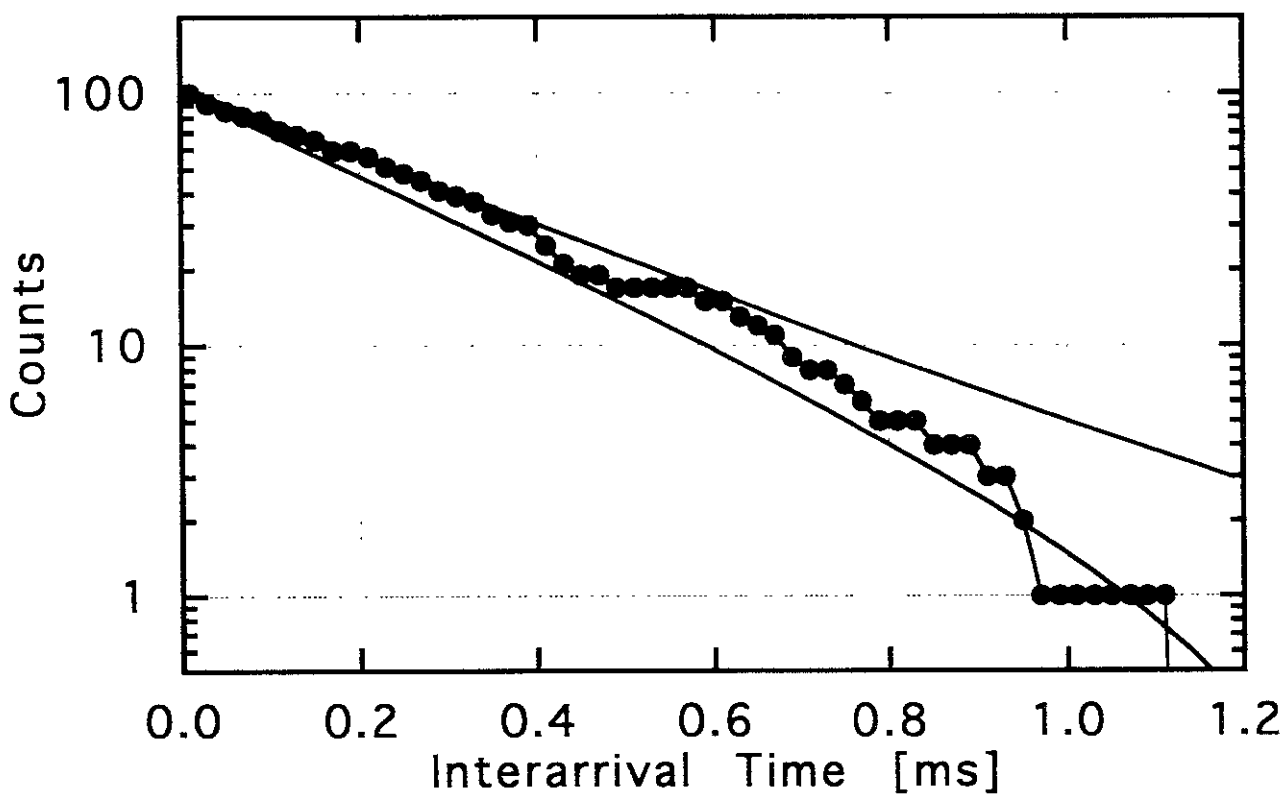

Fig. 9

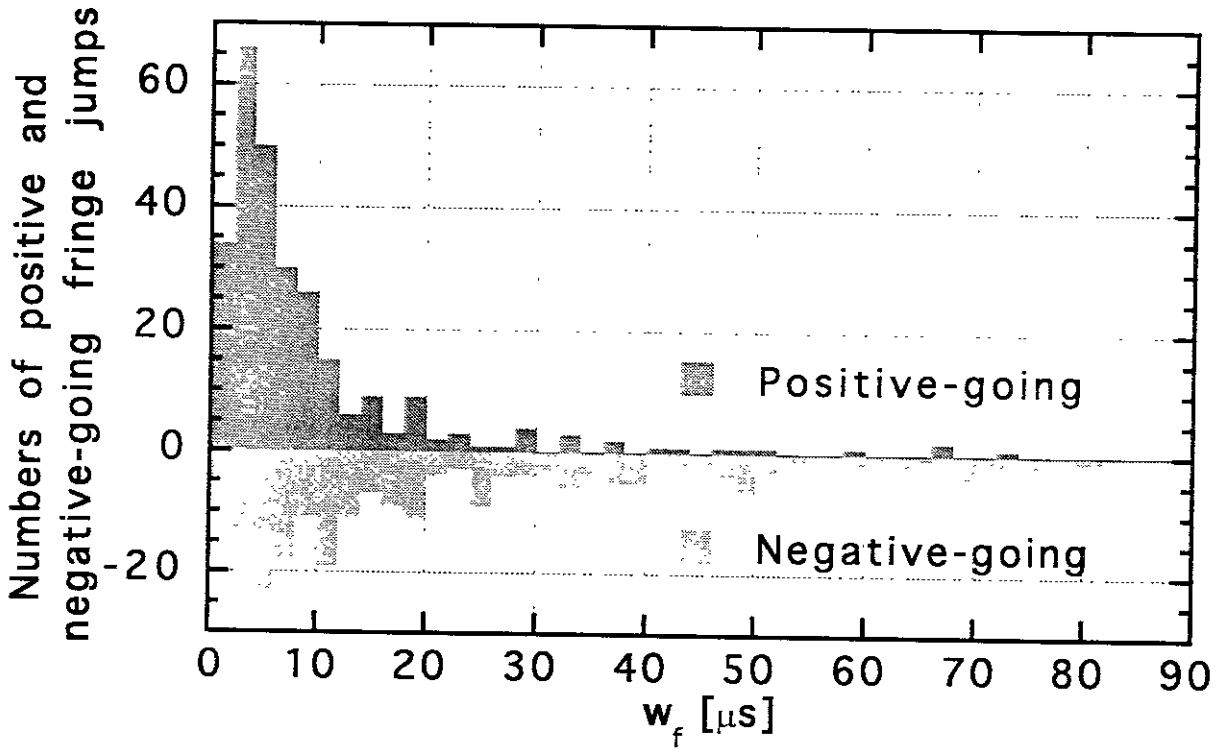
Numbers of positive and negative-going fringe jumps
60
40
20
0
-20
0
10
20
30
40
50
60
70
80
90
w_f [μs]
Positive-going
Negative-going

Fig. 10

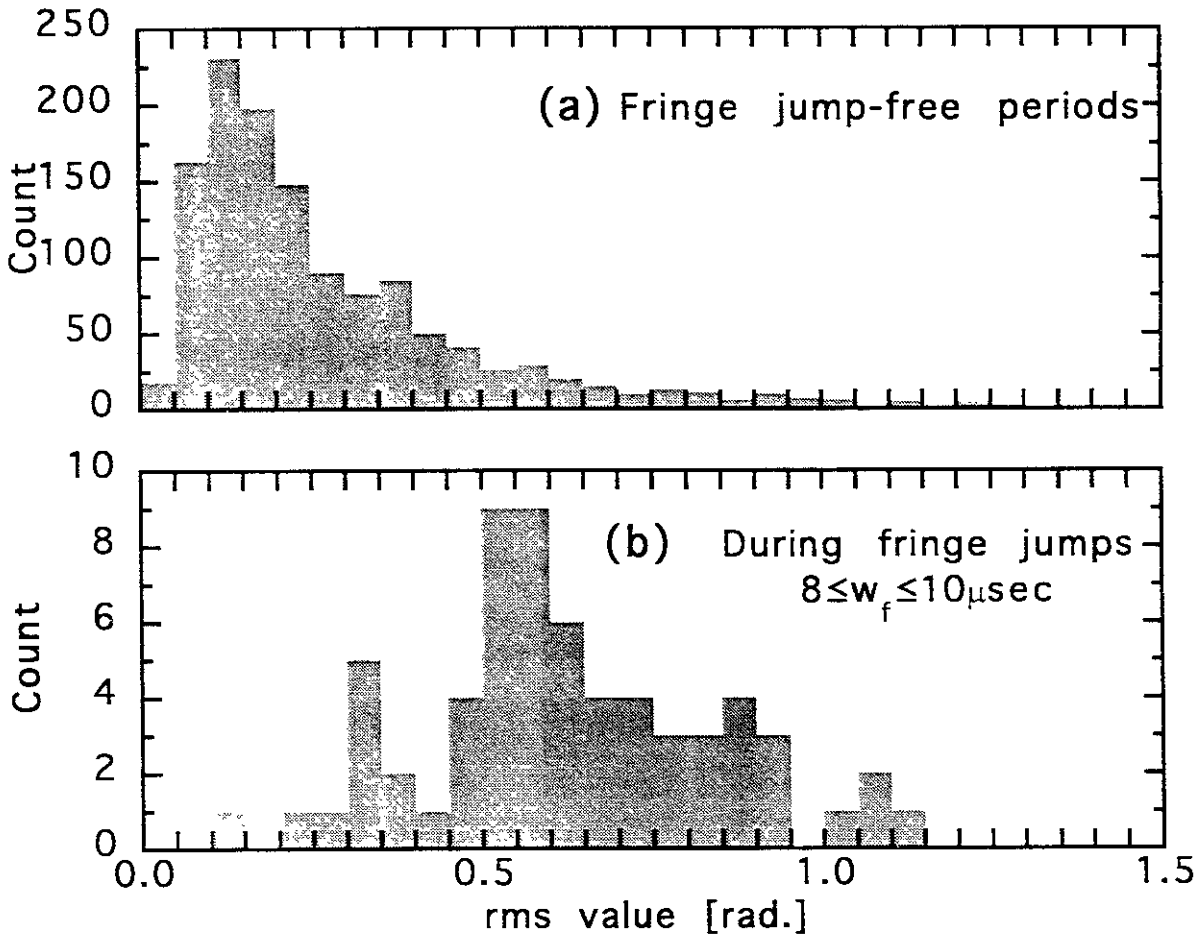
250
200
150
100
50
0
Count
(a) Fringe jump-free periods
10
8
6
4
2
0
Count
(b) During fringe jumps
8≤w_f≤10μsec
0.0
0.5
1.0
1.5
rms value [rad.]

Fig.11

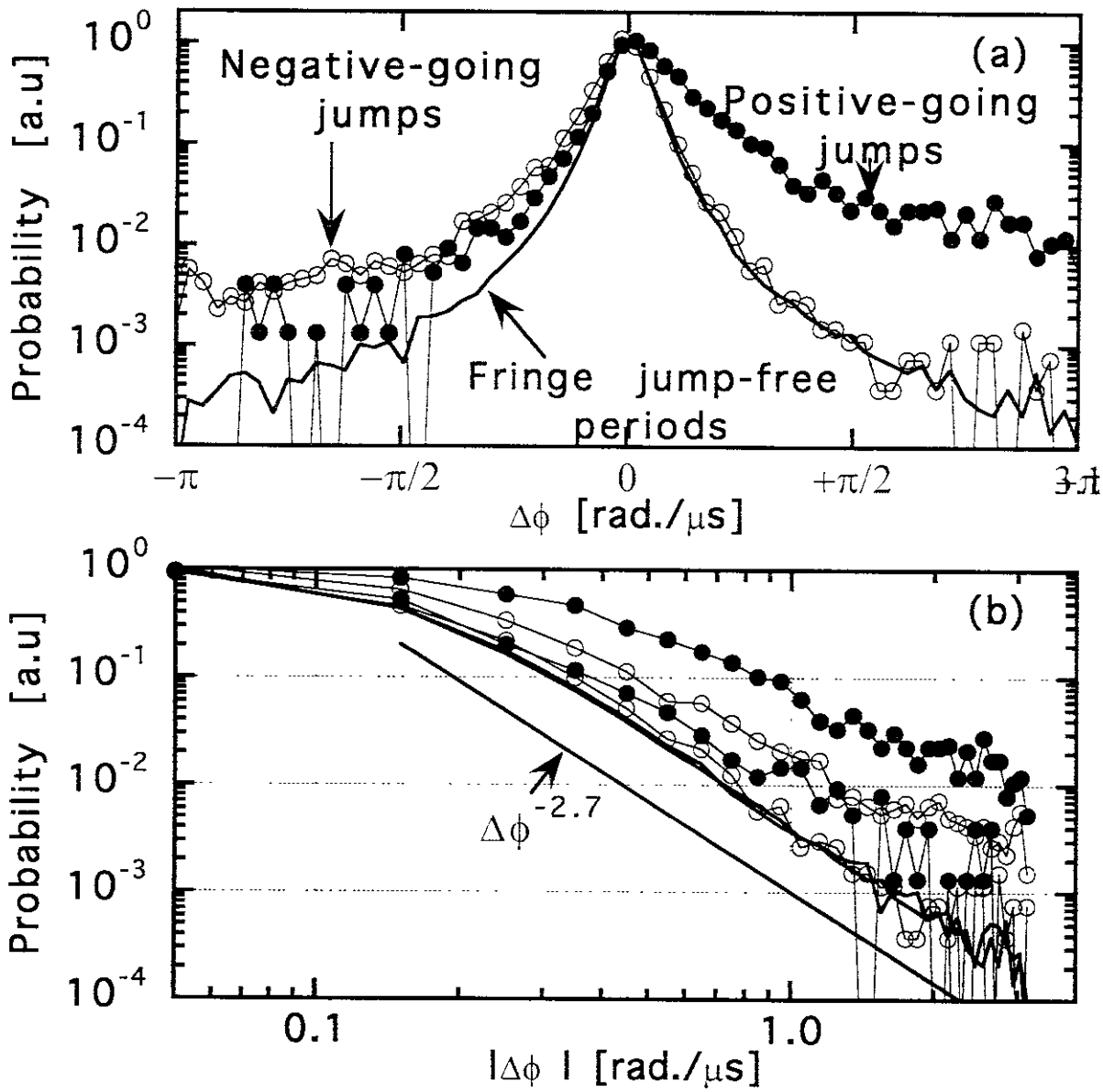
Probability [a.u]
10^0
10^{-1}
10^{-2}
10^{-3}
10^{-4}
Negative-going jumps
(a)
Positive-going jumps
Fringe jump-free periods
$-\pi$
$-\pi/2$
0
$+\pi/2$
3π
$\Delta\phi$ [rad./μs]
Probability [a.u]
(b)
$\Delta\phi^{-2.7}$
0.1
1.0
$|\Delta\phi|$ [rad./μs]

Fig.12

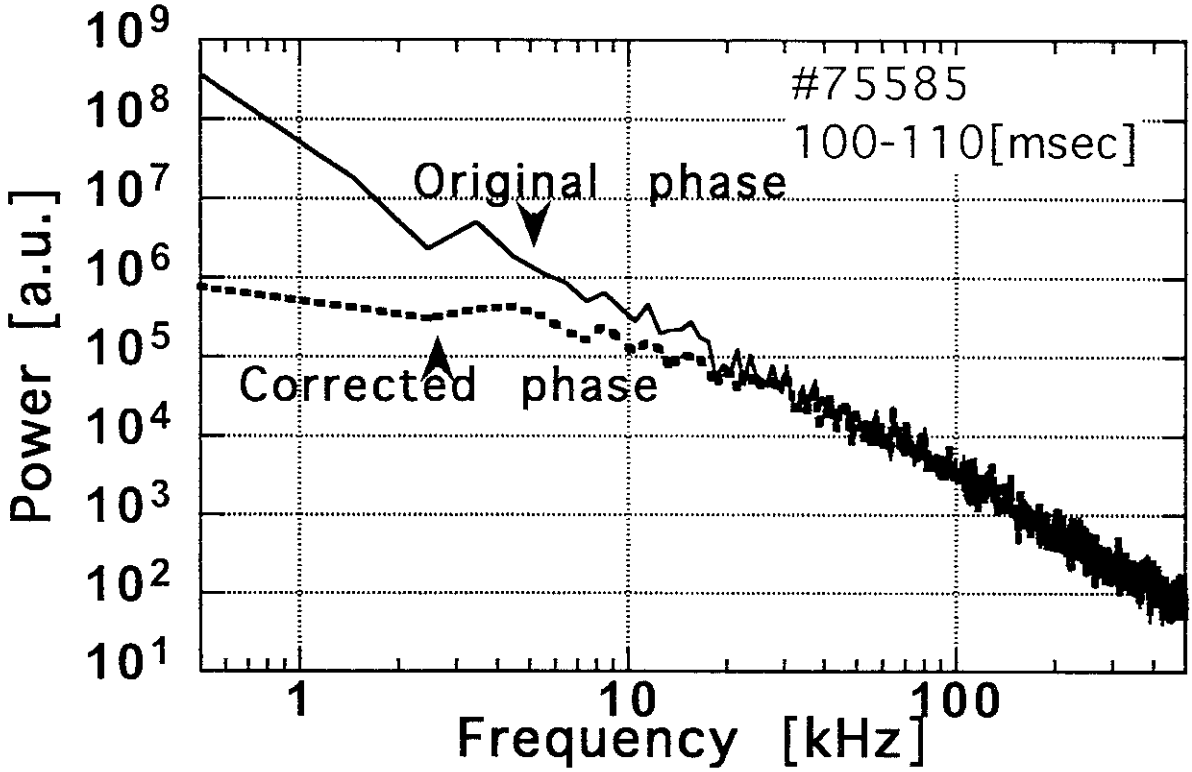
#75585
100-110[msec]
Original phase
Corrected phase
Power [a.u.]
Frequency [kHz]
10^9
10^8
10^7
10^6
10^5
10^4
10^3
10^2
10^1
1
10
100

Fig.13

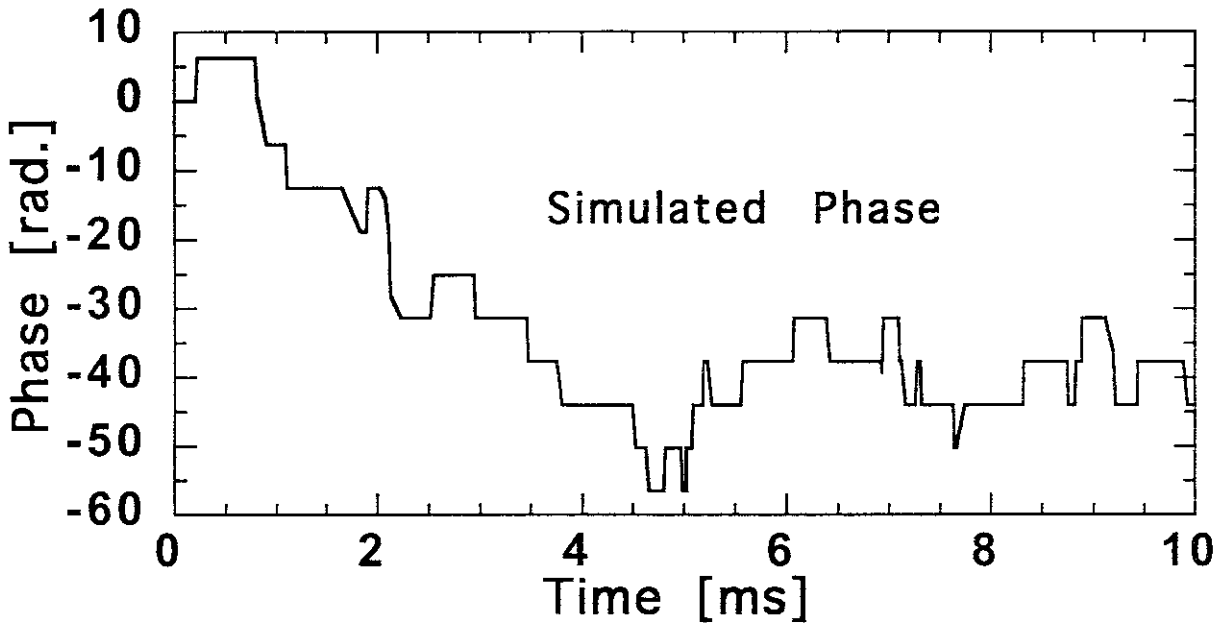
10
0
-10
-20
-30
-40
-50
-60
Phase [rad.]
Simulated Phase
0
2
4
6
8
10
Time [ms]

Fig. 14

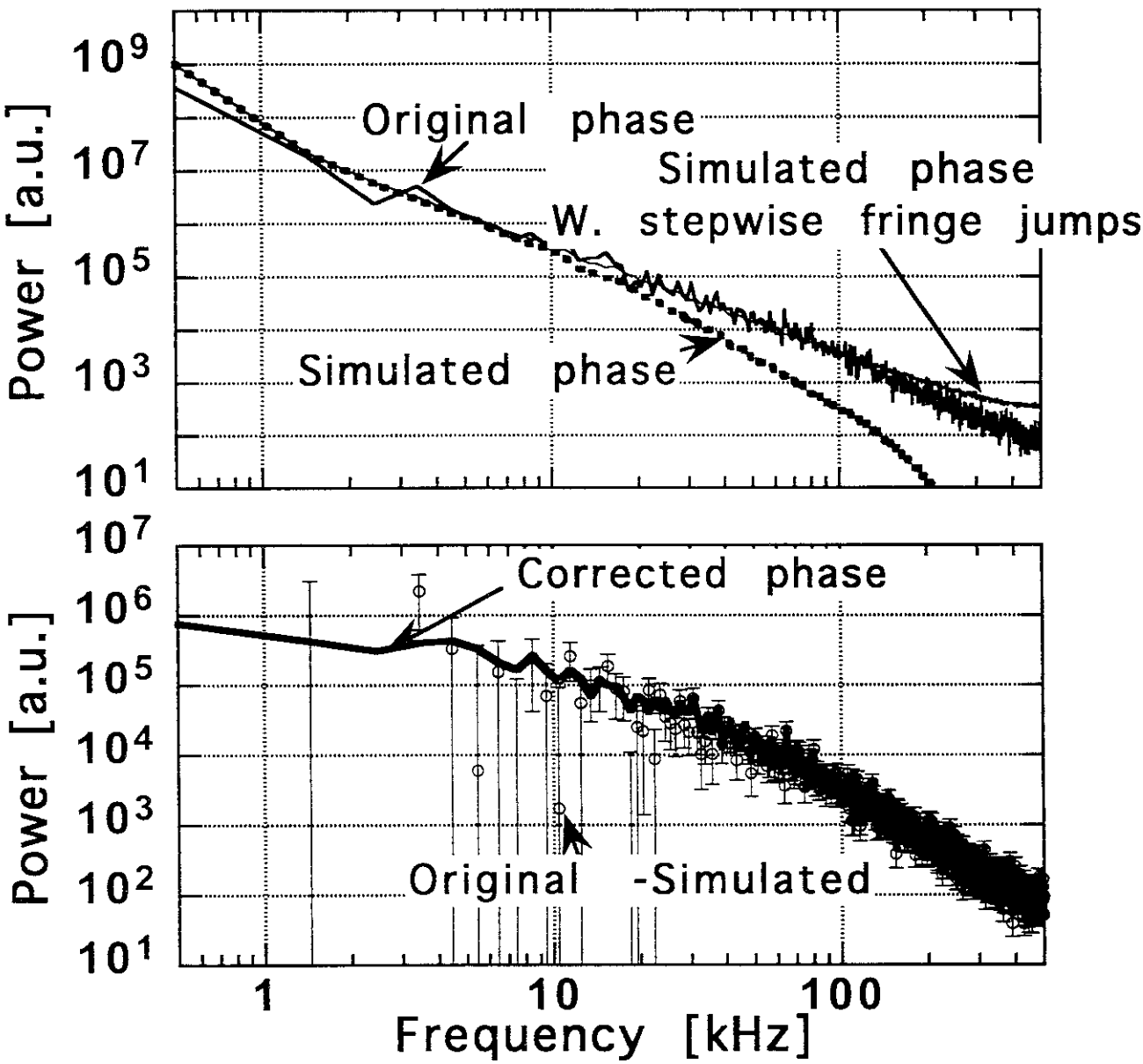
Power [a.u.]
10^9
10^7
10^5
10^3
10^1
Original phase
Simulated phase
W. stepwise fringe jumps
Simulated phase
Power [a.u.]
10^7
10^6
10^5
10^4
10^3
10^2
10^1
Corrected phase
Original -Simulated
1
10
100
Frequency [kHz]

Fig.15

Recent Issues of NIFS Series

NIFS-446 S. Murakami, N. Nakajima, S. Okamura, M. Okamoto and U. Gasparino,
Orbit Effects of Energetic Particles on the Reachable β–Value and the Radial Electric Field in NBI and ECR Heated Heliotron Plasmas; Sep. 1996 (IAEA-CN-64/CP -6) Sep. 1996

NIFS-447 K. Yamazaki, A. Sagara, O. Motojima. M. Fujiwara, T. Amano, H. Chikaraishi. S. Imagawa, T. Muroga, N. Noda, N. Ohyabu, T. Satow, J.F. Wang, K.Y. Watanabe. J. Yamamoto . H. Yamanishi, A. Kohyama, H. Matsui, O. Mitarai, T. Noda, A.A. Shishkin, S. Tanaka and T. Terai
Design Assessment of Heliotron Reactor; Sep. 1996 (IAEA-CN-64/G1-5)

NIFS-448 M. Ozaki, T. Sato and the Complexity Simulation Group,
Interactions of Convecting Magnetic Loops and Arcades; Sep. 1996

NIFS-449 T. Aoki,
Interpolated Differential Operator (IDO) Scheme for Solving Partial Differential Equations; Sep. 1996

NIFS-450 D. Biskamp and T. Sato,
Partial Reconnection in the Sawtooth Collapse; Sep. 1996

NIFS-451 J. Li, X. Gong, L. Luo, F.X. Yin, N. Noda, B. Wan, W. Xu, X. Gao, F. Yin, J.G. Jiang, Z. Wu., J.Y. Zhao, M. Wu, S. Liu and Y. Han,
Effects of High Z Probe on Plasma Behavior in HT-6M Tokamak; Sep. 1996

NIFS-452 N. Nakajima, K. Ichiguchi, M. Okamoto and R.L. Dewar,
Ballooning Modes in Heliotrons/Torsatrons; Sep. 1996 (IAEA-CN-64/D3-6)

NIFS-453 A. Iiyoshi,
Overview of Helical Systems; Sep. 1996 (IAEA-CN-64/O1-7)

NIFS-454 S. Saito, Y. Nomura, K. Hirose and Y.H. Ichikawa,
Separatrix Reconnection and Periodic Orbit Annihilation in the Harper Map; Oct. 1996

NIFS-455 K. Ichiguchi, N. Nakajima and M. Okamoto,
Topics on MHD Equilibrium and Stability in Heliotron / Torsatron; Oct. 1996

NIFS-456 G. Kawahara, S. Kida, M. Tanaka and S. Yanase,
Wrap, Tilt and Stretch of Vorticity Lines around a Strong Straight Vortex Tube in a Simple Shear Flow; Oct. 1996

NIFS-457 K. Itoh, S.- I. Itoh, A. Fukuyama and M. Yagi,
Turbulent Transport and Structural Transition in Confined Plasmas; Oct. 1996

NIFS-458 A. Kageyama and T. Sato,
Generation Mechanism of a Dipole Field by a Magnetohydrodynamic Dynamo; Oct. 1996

NIFS-459 K. Araki, J. Mizushima and S. Yanase,
The Non-axisymmetric Instability of the Wide-Gap Spherical Couette Flow; Oct. 1996

NIFS-460 Y. Hamada, A. Fujisawa, H. Iguchi, A. Nishizawa and Y. Kawasumi,
A Tandem Parallel Plate Analyzer; Nov. 1996

NIFS-461 Y. Hamada, A. Nishizawa. Y. Kawasumi, A. Fujisawa, K. Narihara. K. Ida, A. Ejiri, S. Ohdachi, K. Kawahata, K. Toi. K. Sato, T. Seki, H. Iguchi, K. Adachi. S. Hidekuma, S.Hirokura, K. Iwasaki, T. Ido, M. Kojima, J. Koong, R. Kumazawa, H. Kuramoto, T. Minami, I. Nomura, H. Sakakita, M. Sasao, K.N. Sato, T. Tsuzuki, J. Xu, I. Yamada and T. Watari,
Density Fluctuation in JIPP T-IIU Tokamak Plasmas Measured by a Heavy Ion Beam Probe; Nov. 1996

NIFS-462 N. Katsuragawa, H. Hojo and A. Mase,
Simulation Study on Cross Polarization Scattering of Ultrashort-Pulse Electromagnetic Waves; Nov. 1996

NIFS-463 V. Voitsenya, V. Konovalov. O. Motojima, K. Narihara, M. Becker and B. Schunke,
Evaluations of Different Metals for Manufacturing Mirrors of Thomson Scattering System for the LHD Divertor Plasma; Nov. 1996

NIFS-464 M. Pereyaslavets, M. Sato, T. Shimozuma, Y. Takita, H. Idei, S. Kubo, K. Ohkubo and K. Hayashi,
Development and Simulation of RF Components for High Power Millimeter Wave Gyrotrons; Nov. 1996

NIFS-465 V.S. Voitsenya, S. Masuzaki, O. Motojima, N. Noda and N. Ohyabu,
On the Use of CX Atom Analyzer for Study Characteristics of Ion Component in a LHD Divertor Plasma; Dec. 1996

NIFS-466 H. Miura and S. Kida,
Identification of Tubular Vortices in Complex Flows; Dec. 1996

NIFS-467 Y. Takeiri, Y. Oka, M. Osakabe, K. Tsumori, O. Kaneko, T. Takanashi, E. Asano, T. Kawamoto, R. Akiyama and T. Kuroda,
Suppression of Accelerated Electrons in a High-current Large Negative Ion Source; Dec. 1996

NIFS-468 A. Sagara, Y. Hasegawa, K. Tsuzuki, N. Inoue, H. Suzuki, T. Morisaki, N. Noda, O. Motojima, S. Okamura, K. Matsuoka, R. Akiyama, K. Ida, H. Idei, K. Iwasaki, S. Kubo, T. Minami, S. Morita, K. Narihara, T. Ozaki, K. Sato, C. Takahashi, K. Tanaka, K. Toi and I. Yamada,
Real Time Boronization Experiments in CHS and Scaling for LHD; Dec.

1996

NIFS-469 V.L. Vdovin, T.Watari and A. Fukuyama,
3D Maxwell-Vlasov Boundary Value Problem Solution in Stellarator Geometry in Ion Cyclotron Frequency Range (final report); Dec. 1996

NIFS-470 N. Nakajima, M. Yokoyama, M. Okamoto and J. Nührenberg,
Optimization of M=2 Stellarator; Dec. 1996

NIFS-471 A. Fujisawa, H. Iguchi. S. Lee and Y. Hamada,
Effects of Horizontal Injection Angle Displacements on Energy Measurements with Parallel Plate Energy Analyzer; Dec. 1996

NIFS-472 R. Kanno, N. Nakajima, H. Sugama, M. Okamoto and Y. Ogawa,
Effects of Finite-β and Radial Electric Fields on Neoclassical Transport in the Large Helical Device; Jan. 1997

NIFS-473 S. Murakami, N. Nakajima, U. Gasparino and M. Okamoto,
Simulation Study of Radial Electric Field in CHS and LHD; Jan. 1997

NIFS-474 K. Ohkubo. S. Kubo, H. Idei, M. Sato, T. Shimozuma and Y. Takita,
Coupling of Tilting Gaussian Beam with Hybrid Mode in the Corrugated Waveguide; Jan. 1997

NIFS-475 A. Fujisawa, H. Iguchi, S. Lee and Y. Hamada,
Consideration of Fluctuation in Secondary Beam Intensity of Heavy Ion Beam Prove Measurements; Jan. 1997

NIFS-476 Y. Takeiri, M. Osakabe, Y. Oka, K. Tsumori, O. Kaneko, T. Takanashi, E. Asano, T. Kawamoto, R. Akiyama and T. Kuroda,
Long-pulse Operation of a Cesium-Seeded High-Current Large Negative Ion Source; Jan. 1997

NIFS-477 H. Kuramoto, K. Toi, N. Haraki, K. Sato, J. Xu, A. Ejiri, K. Narihara, T. Seki, S. Ohdachi, K. Adati, R. Akiyama, Y. Hamada, S. Hirokura, K. Kawahata and M. Kojima,
Study of Toroidal Current Penetration during Current Ramp in JIPP T-IIU with Fast Response Zeeman Polarimeter; Jan., 1997

NIFS-478 H. Sugama and W. Horton,
Neoclassical Electron and Ion Transport in Toroidally Rotating Plasmas; Jan. 1997

NIFS-479 V.L. Vdovin and I.V. Kamenskij,
3D Electromagnetic Theory of ICRF Multi Port Multi Loop Antenna; Jan. 1997

NIFS-480 W.X. Wang, M. Okamoto, N. Nakajima, S Murakami and N. Ohyabu,
Cooling Effect of Secondary Electrons in the High Temperature Divertor Operation; Feb. 1997

NIFS-481 K. Itoh, S.-I. Itoh. H. Soltwisch and H.R. Koslowski,
Generation of Toroidal Current Sheet at Sawtooth Crash; Feb. 1997

NIFS-482 K. Ichiguchi,
Collisionality Dependence of Mercier Stability in LHD Equilibria with Bootstrap Currents; Feb. 1997

NIFS-483 S. Fujiwara and T. Sato,
Molecular Dynamics Simulations of Structural Formation of a Single Polymer Chain: Bond-orientational Order and Conformational Defects; Feb. 1997

NIFS-484 T. Ohkawa,
Reduction of Turbulence by Sheared Toroidal Flow on a Flux Surface; Feb. 1997

NIFS-485 K. Narihara, K. Toi, Y. Hamada, K. Yamauchi, K. Adachi, I. Yamada, K. N. Sato, K. Kawahata, A. Nishizawa, S. Ohdachi, K. Sato, T. Seki. T. Watari, J. Xu, A. Ejiri, S. Hirokura, K. Ida. Y. Kawasumi, M. Kojima, H. Sakakita, T. Ido. K. Kitachi. J. Koog and H. Kuramoto,
Observation of Dusts by Laser Scattering Method in theJIPPT-IIU Tokamak Mar. 1997

NIFS-486 S. Bazdenkov, T. Sato and The Complexity Simulation Group,
Topological Transformations in Isolated Straight Magnetic Flux Tube; Mar. 1997

NIFS-487 M. Okamoto.
Configuration Studies of LHD Plasmas; Mar. 1997

NIFS-488 A. Fujisawa, H. Iguchi, H. Sanuki, K. Itoh, S. Lee, Y. Hamada, S. Kubo, H. Idei, R. Akiyama, K. Tanaka, T. Minami, K. Ida, S. Nishimura, S. Morita, M. Kojima, S. Hidekuma. S.-I. Itoh, C. Takahashi, N. Inoue, H. Suzuki, S. Okamura and K. Matsuoka,
Dynamic Behavior of Potential in the Plasma Core of the CHS Heliotron/Torsatron; Apr. 1997

NIFS-489 T. Ohkawa,
Pfirsch - Schlüter Diffusion with Anisotropic and Nonuniform Superthermal Ion Pressure; Apr. 1997

NIFS-490 S. Ishiguro and The Complexity Simulation Group,
Formation of Wave-front Pattern Accompanied by Current-driven Electrostatic Ion-cyclotron Instabilities; Apr. 1997

NIFS-491 A. Ejiri, K. Shinohara and K. Kawahata,
An Algorithm to Remove Fringe Jumps and its Application to Microwave Reflectometry; Apr. 1997